Small Structures

www.small-structures.com

RESEARCH ARTICLE OPEN ACCESS

Focused Thermal Emission From a Radiative Metasurface

Tsuyoshi Kawaida[1] | Kazuki Wada[1] | Kazuma Sekiya[1] | Megumi Tanaka[1] | Thoko Ogata[2] | Yasutaka Matsuo[2] | Saulius Juodkazis[3,4,5] | Yoshiaki Nishijima[1,4,6,7]

[1]Department of Electrical and Computer Engineering, Graduate School of Engineering, Yokohama National University, Yokohama, Kanagawa, Japan | [2]Research Institute for Electronic Science, Hokkaido University, Sapporo, Hokkaido, Japan | [3]Optical Sciences Centre, Swinburne University of Technology, Hawthorn, Victoria, Australia | [4]Institute of Advanced Sciences, Yokohama National University, Yokohama, Kanagawa, Japan | [5]Laser Research Centre, Physics Faculty, Vilnius University, Vilnius, Lithuania | [6]Institute for Multidisciplinary Sciences, Yokohama National University, Yokohama, Kanagawa, Japan | [7]PRESTO, JST, Japan

Correspondence: Saulius Juodkazis (sjuodkazis@swin.edu.au) | Yoshiaki Nishijima (nishijima-yoshiaki-sp@ynu.ac.jp)

Received: 30 September 2025 | **Revised:** 22 January 2026 | **Accepted:** 26 January 2026

Keywords: focusing radiation | infrared light source | metalens | metasurface | mid-infrared | radiation control | thermal radiation

ABSTRACT

In the field of mid-infrared (m-IR) applications, a need exists to control thermal radiation from metal-insulator-metal (MIM) metasurfaces without any additional optical components. Here, we introduce the metalens concept for radiation control from MIM metasurfaces. A finite-difference time-domain (FDTD) simulation is used to design the radiative metasurface to focus its thermal radiation. Electron-beam lithography is implemented to fabricate a 5-mm-diameter radiative metalens. Experiments to measure the thermal radiation from metasurfaces validate the focusing performance of the metalens by direct measurement of the 3D spatial distribution of thermal radiation. These findings form the basis for engineering metasurfaces for focusing thermal radiation and can be applied in areas such as gas sensor design, semiconductor device cooling, and energy harvesting.

1 | Introduction

Thermal radiation from a metal-insulator-metal (MIM) metasurface is a promising and efficient light source in the mid-infrared (m-IR) range. However, the thermal radiation emitted from the MIM metasurface produces light that spreads at ≈120°. For non-dispersive infrared absorption (NDIR) applications, the infrared light should be efficiently guided to the m-IR detectors. If thermal radiation spreads at 120°, most of the radiated energy becomes lost for the detectors, even though their photothermal energy conversion efficiency could be close to 100%.

A simple resolution of this problem is to introduce an optical lens in the m-IR system. Materials such as Si, CaF_2, sapphire (up to $\lambda \sim 5$ μm), and ZnSe can be used for the optical components at m-IR wavelengths. However, micromachining and fabricating micro-optical elements from these materials are challenging because of the brittle nature of the crystals. In addition, these materials have a high refractive index of $n = (2 \sim 3)$, which makes fabricated lenses, mirrors, or any other optical elements less efficient because of the high reflection losses in the m-IR range. Indeed, reflection from the polished surface (in air) $R = [(n-1)/(n+1)]^2 \sim 0.3$ is estimated for a refractive index of $n = 3.5$ (Si). Therefore, it is necessary to realize the focusing function without any optical components, that is, focusing should be provided by a free surface.

Antireflective coating can reduce the reflection loss. However, in the m-IR wavelength region, broadband antireflective coating is realized only by complex multiple coatings such as Ge (high refractive index), ZnS (middle refractive index), YF_3 (low refractive index), and Y_2O_3 (adhesion layer) [1]. Such antireflective coatings make fabrication complex.

Another way to control thermal radiation is to use metals for MIM metasurfaces. A metalens is a diffractive optical element that can control the wavefront by the transmission phase shift of each meta-atom [2–16]. These studies show the use of transparent dielectric materials and transparent focusing apertures, but the metalens concept should be applied not only to the

Small Structures, 2026; 7:e202500695
https://doi.org/10.1002/sstr.202500695

transparent metalenses but also to reflective or radiative materials. The basic idea to focus thermal radiation from the surface is suggested by the design of the Fresnel lens and Fresnel zone plate (FZP). In the case of MIM metasurfaces, the ability to control the phase of thermal radiation would provide focusing at the designed focal length.

In this study, we developed a metasurface that realizes perfect absorption (no reflectance) and, hence, efficient thermal radiation focused using a MIM metalens. The metal structure of the metalens has a Cr absorption layer and MIM sandwich on top: a 100 nm Au film, 100 nm SiO_2, and 50 nm-thick Au microdiscs. We demonstrated realization of spectrally narrow thermal radiation using the coupling between the plasmon resonance of the disc pattern and the continuous metal film of the MIM metasurface. Such coupling can be utilized in applications such as NDIR gas sensors.

Figure 1 illustrates the concept of thermal radiation generated by conventional and metalens-MIM metasurfaces. With phase control, an arbitrary focal length can be set where the detector is placed. The light-detection efficiency becomes higher for the focused radiation in the m-IR range.

2 | Experimental: Design, Fabrication, and Characterization

2.1 | Theory and Design of the Radiative Metalens

The metalens concept is based on the phase pattern of the Fresnel lens or FZP. The Fresnel lens is a spherical lens divided into concentric areas. It has a sawtooth cross-section; hence, the phase ramps are used to reduce the thickness of the lens. This is still a refraction-type lens. When the thickness of the Fresnel lens evolves into binary transmission and nontransmission flat segments, that is, of a cocentric lens, it becomes a FZP, which is a diffractive optical element. A metalens has grayscale phase ramps in a ring pattern based on the Fresnel lens design. Both transmission and reflection types of metalenses have been studied previously [7, 17].

The proposed radiative metalens has no transmission characteristics because of its MIM structure. The proposed radiative metalens was designed using the same approach as that used for transparent metalenses based on a pattern of meta-atoms. First, a single meta-atom was simulated using the finite-difference time-domain (FDTD) method (FDTD; Ansys-Lumerical). Because it is not possible to simulate the thermal radiation phase by FDTD, the reflection phase was used instead. The absorption of the MIM metasurface was analyzed from the reflection spectra, which were used to account for the amplitude and phase changes. The direction z was set as the direction of propagation of the incident light, and the lateral size of the meta-atom in the x and y directions was set to 3 μm. The boundary conditions in the x, y, and z dimensions were set as perfectly matching layers (PMLs). The mesh was set as auto nonuniform with an accuracy of 1 because of the limitation of simulation memory.

The phase map for Fresnel lens realization is [3]

$$\Delta\phi(x,y) = \phi(x,y,\lambda) - \phi(0,0,\lambda) = -\frac{2\pi}{\lambda}\left(\sqrt{(x^2+y^2+f^2)} - f\right) \tag{1}$$

where ϕ is the phase, λ is the wavelength for which the phase pattern is designed, and f is the focal length. Equation (1) is derived from the spherical lens condition, and the Fresnel lens shape is converted to the phase shift.

By using the spherical lens equation, the meta-atoms were arranged into a 2D array. The number of concentric circles N strongly depends on the focal length, f, and the total diameter of the metalens, for example, $N = 119$ ($f = 5$ mm), 81 ($f = 7.5$ mm), and 62 ($f = 10$ mm) in this study.

The complete metalens structure was simulated by FDTD. Because of the memory limitation of the simulation system, the allowed maximum for manageable memory and calculation time requirements was $100 \times 100 \times 100$ μm^3 with accuracy

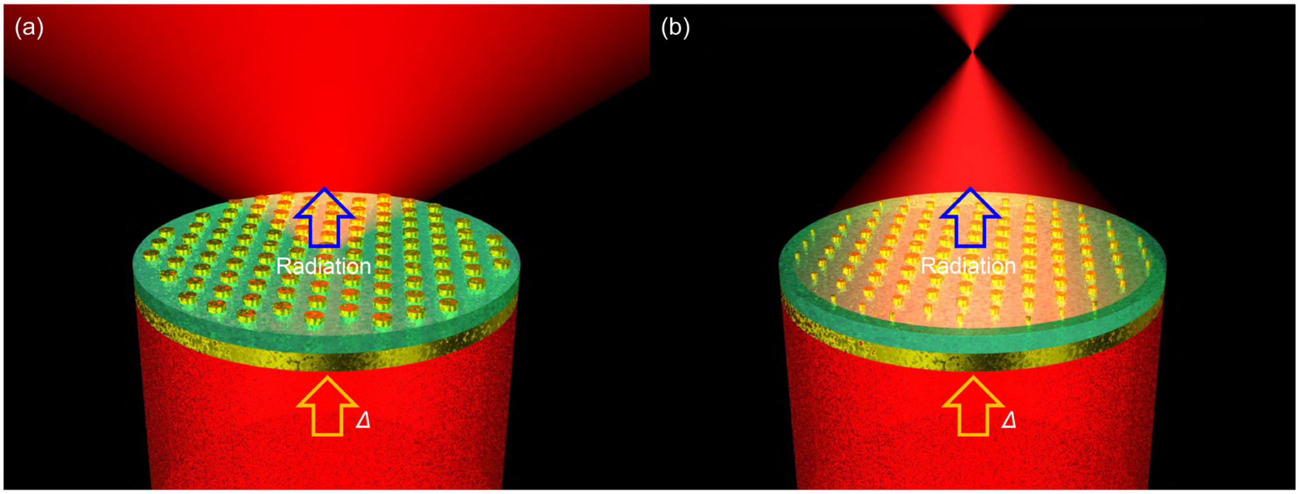

FIGURE 1 | Schematic illustration of thermal radiation from (a) a conventional MIM metasurface and (b) a radiative-metalens metasurface. The black-body radiation is generated by the applied energy (heating) Δ to the MIM metasurface. The angular distribution of the Lambertian black-body radiator surface is cos θ; θ is the angle between the surface normal and the direction of observation.

setting 1, which is the nonuniform mesh setting. The usual ray-tracing method was used for the full metalens simulation. With those settings, the performed calculations for the focal length structures for f from 5 to 10 mm were within a reasonable simulation time (less than 3 days per metalens).

The challenge for the FDTD design of a metalens is calculation of the thermal radiation phase Therefore, the phase of the reflected light was extracted by implementing an external dipole light source.

2.2 | Fabrication of the Radiative Metalens

A 2D array of meta-atoms was converted to a lithography standard GDSII file [18]. The pattern of disc meta-atoms was exposed using an electron (e-) beam drawing system onto the sample. The sample was layers of 200 nm of Au deposited on a Si substrate with 150 nm of SiO_2 deposited on top; a 5 nm Cr layer was used as the adhesion layer between gold and SiO_2. The e-beam drawing was performed on the EB resist (AR-P 6200, ALLRESIST), which had a thickness of 400 nm when spin coated at 4000 rpm on the SiO_2 substrate. The metasurface of disc meta-atoms was exposed and developed for subsequent deposition of 50 nm of Au on a 5 nm Cr adhesion layer. After lift-off, the final MIM pattern or Fresnel lens was obtained. This is the standard fabrication method for MIM metasurfaces.

The MIM metasurface must be large enough to measure thermal radiation. We designed the metasurface over a 5-mm diameter. The focal length f was set to 5, 7.5, and 10 mm for the fabricated samples.

2.3 | Measurement of Thermal Radiation

Thermal radiation was measured using a lab-assembled measurement setup. A schematic illustration of the setup is shown in Figure 2. The piezoheater was fixed onto an x, y, z triaxis stage. The stage and heater were covered with aluminum foil to remove the thermal radiation noise from the other parts of the system. Only the metasurface sample had an exposure opening in the Al screen for measurements. The radiative metasurface sample was fixed onto the heater with thermally conductive paste. The radiation was collected using a reflection lens (Thorlabs, LMN15X-UVV, 15×, numerical aperture NA = 0.3, focal length 13.3 mm, and back-focal length of infinity).

3 | Results and Discussion

3.1 | Numerical Modeling of the Phase Range

Figure 3a shows the optical reflection spectra simulated by FDTD for different disc diameters. The simple square lattice of a single meta-atom was used for simulations. The x and y spans of the simulation region were set to 3 µm, and the maximum disc diameter was 2.8 µm. If the disc diameter becomes 3 µm, it connects to a neighboring disc according to the periodic boundary conditions. Such a condition is incompatible with the proposed metasurface design of individual meta-atoms and was not investigated.

When the disc diameter changed from 1.6 to 2.0 µm, a strong change in the phase of reflected light of $\lambda = 5$ µm wavelength occurred. Therefore, this range was simulated with increased resolution using disc diameter increments of 0.02 µm. Figure 3b shows the reflected light phase ϕ and reflectance R spectra versus disc diameter. More than 2π phase change occurred in the wavelength region from 1.0 to 3.0 µm. The strongest phase change $\Delta\phi$ was at the strong plasmon resonance region of disc diameters from 1.4 to 1.8 µm. The reflection phase was obtained using S-parameters in the FDTD simulation [19, 20]. In the series of meta-atom (disc) simulations, an almost 2π reflected phase change was obtained using a disc diameter in a narrower range from 1.3 to 2.4 µm. The inflection point of the sigmoid shape was matched to the minimum reflection near the 1.8 µm disc diameter (Figure 3b).

Figure 4a shows the optical phase pattern of a spherical metalens obtained from Equation (1) . In Figure 4b, the complete metalens simulation design for the focal length was set to 75 µm with a disc array region of 100 µm in cross section. Simulation results showed that reflected light was focused at ≈70 µm from the metasurface, confirming the expected behavior of the metalens.

Next, the radiative metalens structures were simulated for thermal radiation performance. Figure 4b,c show the large-area

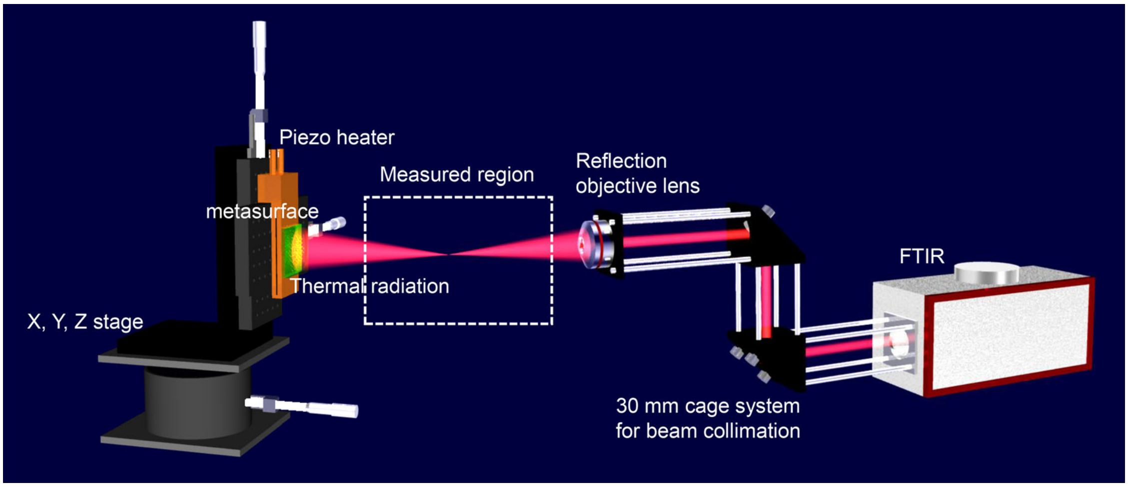

FIGURE 2 | Optical setup of the assembled radiation measurement system using an x, y, z stage, reflection objective lens, and compact FTIR spectrometer.

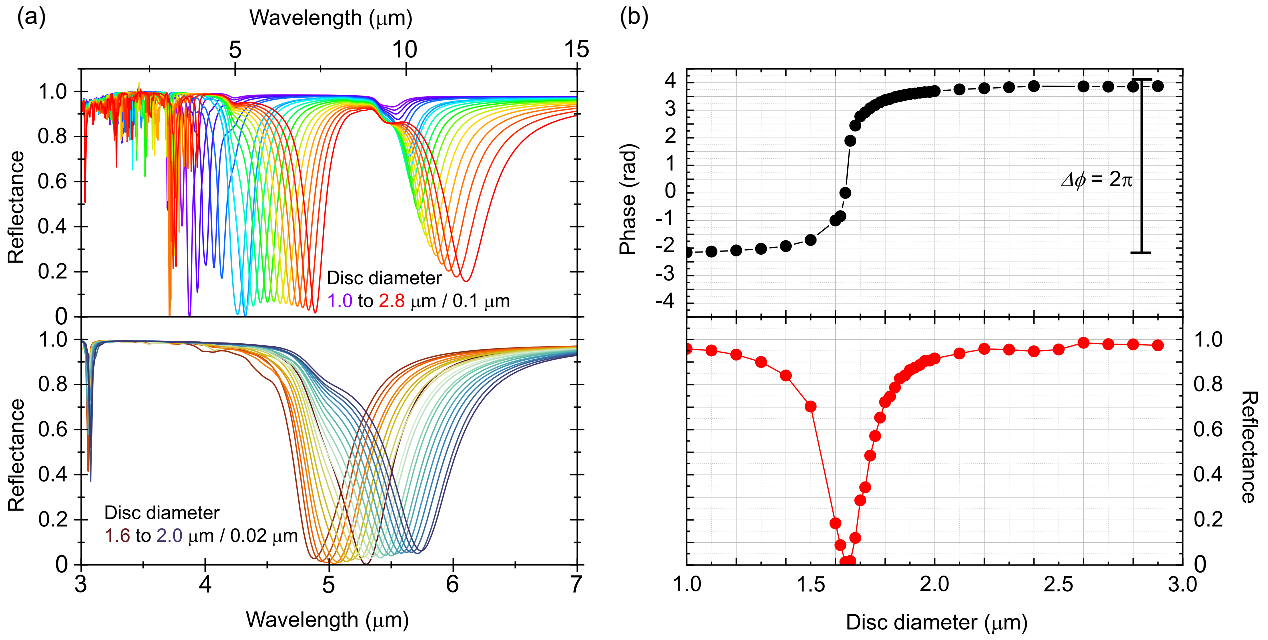

FIGURE 3 | (a) Reflection spectra of meta-atoms with disc diameters from 1.0 to 2.8 μm with a step of 0.1 μm (upper panel) and 1.6 to 2.0 μm with a smaller 0.02 μm step (lower panel). (b) Plot of the phase (upper panel) and reflectance R (lower panel) from the meta-atom at $\lambda = 5$ μm wavelength.

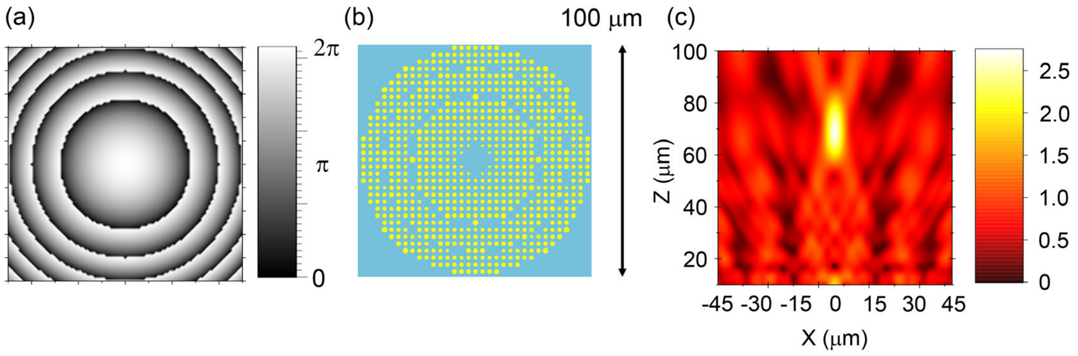

FIGURE 4 | (a) Reflection phase mapping calculated using the spherical lens equation, Equation (1) . The focal length was set to $f = 75$ μm. (b) GDSII file pattern of nano-disc mapping with a 100×100 μm^2 region; lens diameter $D = 100$ μm. (c) Reflection $|E|$-field image of the axial cross-section simulated with FDTD using the calculated GDSII files; $\lambda = 5$ μm. The f-number $f_{\#} \equiv f/D \approx 75/100 = 0.75$, which corresponds to the numerical aperture $NA = 1/(2f_{\#}) = 0.67$.

FDTD simulation of reflection using the full metalens array. The simulation size was nearly at the limit of our workstation's capabilities. The results show that the reflection light was focused at ≈70 μm from the surface, which agrees with the designed value and validates the design. To experimentally demonstrate thermal radiation focusing, the focal length and diameter were increased.

3.2 | Numerical Modeling of Chromatic Aberrations

Characterization of chromatic aberration is essential for understanding the optical performance of a metalens. FDTD simulations were performed to monitor the electric-field distribution in the x-z plane across five wavelengths from $\lambda = 4.0$ to 6.0 μm (Figure S1). The focal length decreased from the design value of 75 μm (at $\lambda = 5.0$ μm) to 60 μm at $\lambda = 5.5$ μm and 55 μm at $\lambda = 6.0$ μm. From these trends, the focal points for 4.0 and 4.5 μm were expected to fall outside the simulation window. Minor intensity spots within the simulation domain are attributed to higher-order diffraction. Unlike conventional refractive lenses, where chromatic aberration is driven by material dispersion (typically resulting in longer focal lengths and longer wavelengths), the chromatic response of this radiative metalens was dictated by the interplay between the wavelength and the phase characteristics of the meta-atoms, as formulated by Equation (1) .

Figure S2 shows the focusing performance evaluated by FDTD simulations by transitioning from a plane wave to a Gaussian beam. Utilizing Ansys Lumerical FDTD software, the full-width at half-maximum (FWHM) of the Gaussian source was systematically varied. A plane wave is physically equivalent to a Gaussian wave with an infinite FWHM. Hence, the results for sufficiently large FWHMs should converge with those of plane-wave excitation. In this analysis, the FWHM was varied between one, two, and three times the dimensions of the FDTD calculation domain. Even at a FWHM of three times the domain size, the intensity profile remained slightly nonuniform between the center and the boundaries; nevertheless, the focusing efficiency remained comparable to that of the plane wave. However, a progressive decline in focusing efficiency was observed as the FWHM decreased. This trend indicates that the meta-atoms located near the center of the metalens exert a dominant influence on the overall emission and focusing characteristics.

The focal length f of a FZP is given by the following expression

$$f = \frac{r_1^2}{\lambda} \tag{2}$$

where r_1 represents the radius of the innermost zone, f is the focal length, and λ denotes the wavelength. Since the focal length is inversely proportional to the wavelength, it decreases as the wavelength increases. This behavior, which is consistent with our simulation results, is opposite to that of conventional refractive lenses. In terms of the Abbe number, this lens can be characterized as having a negative Abbe number. While the aforementioned equation describes only the relationship between the diffraction wavelength and the focal position, a standard FZP would concentrate light with uniform intensity across wavelengths, provided the diffraction efficiency remains constant. However, the metalens demonstrated in this study utilizes a focusing phenomenon based on plasmonic resonance and phase shifts. Figure S1b shows the reflection phase shifts and reflection intensities at wavelengths of 4.0, 4.5, 5.0, 5.5, and 6.0 μm. These plots correspond to the results shown in Figure 3 evaluated at different wavelengths. According to these results, the phase coverage remains nearly constant across the wavelengths investigated. However, the reflection intensity and its FWHM vary. At a wavelength of 4 μm, the reflection intensity is higher compared to 5 μm, suggesting superior radiation characteristics. Nevertheless, due to its narrow FWHM, only a limited number of structures can achieve such performance. Conversely, at 6 μm, the radiation uniformity is high due to the broad FWHM, but the high reflectivity results in low overall emissivity.These variations occur because the dielectric thickness of the metasurface is optimized for a wavelength of 5 μm; consequently, the radiation and collection efficiencies decrease at other wavelengths. Thus, the resonance-based radiation-control metasurface acts as a spatial filter where intensity decreases outside the target wavelength despite the presence of chromatic aberration. This filtering effect represents a significant advantage of the proposed metalens structure.

3.3 | Numerical Modeling of Metalens Focusing vs. Phase and Structure Coverage Ranges

In the design of our MIM structures, a phase range coverage (full range was 2π) of ≈90% was shown to yield excellent light collection. Determining a specific phase range required to maintain high metalens performance is critically important. Therefore, the focusing conditions using FDTD calculations were performed by varying the phase coverage from −π to π. Two distinct methods were used to reduce the phase coverage range from 90% and quantify the lens performance. First, the asymmetric reduction method was used, retaining phases starting from the π side and deleting them from the −π side to step down the coverage range to 80%, 70%, and so on. Second, the symmetric reduction was used, retaining phases symmetrically on both the positive and negative sides, centered around the phase of 0. The data from these numerical investigations are summarized in Figures S3 through S5. Figure S3 shows the schematics of the method for retaining phases from π and the electric-field intensity distribution $|E|$ in the x-z plane for the phase coverage ranging from 90% to 50%. Figure S4 shows the schematics for the symmetric reduction method (centered at 0 rad) and the corresponding $|E|$ distributions for occupancy rates from 90% to 50%. Performance at low phase coverage showed a decrease in $|E|$ at the focal point; however, the focusing was maintained. Consequently, the phase coverage was further reduced to 10%. In the symmetric reduction model, focusing disappeared at 10% phase coverage range. In the structure-retaining phases from π, which were defined as asymmetry, focusing was still observed at 10% and disappeared only when the phase coverage fell to 6% or lower. The plotted results of these findings are shown in Figure S5, which also includes the CAD diagrams used for the FDTD calculations. These diagrams reveal that the physical arrangement of the metal nanostructures differs between the two methods. When the data were replotted by converting “phase coverage range” to “structure coverage range,” the results suggest that light collection vanished when the structure coverage fell below ≈5%.

Across all simulated metalenses, the design that retained structures on the π side of the phase exhibited higher light-collection efficiency, because the −π side consisted of structures with small disc diameters, whereas the π side contained structures with larger discs. Consequently, retaining phases on the π side resulted in a larger surface area and volume of gold than with the symmetric method. This effect likely improved light-collection efficiency by balancing the radiation and scattering efficiencies.

3.4 | Numerical Modeling of Metalens Spectral Performance

Figure S6 shows the reflection spectra at the focal plane. For conventional meta-atoms, the reflectance typically ranges from 0 to 1 (0%–100%), however, in metalens-MIM structures designed for light focusing, values exceeding 100% are observed at the focus point at some wavelengths. For instance, in the symmetric structure with a phase coverage of 10%, where focusing was no longer observed, the reflectance remained below 1. A significant difference between the results for the symmetric and asymmetric structures was observed in the reflectance behavior at 4 and 5.5 μm: Although a decrease in reflectance was observed at these wavelengths in the asymmetric structure, it was absent in the symmetric structure. By this logic, this result suggests that the asymmetric structure failed to achieve focusing near 4 and 5.5 μm. In contrast, the symmetric structure exhibited values exceeding 1 even at these wavelengths, indicating that some degree of focusing characteristics was maintained even at this focal plane. As shown in Figure S5, the asymmetric structure achieved a focal field intensity at 50%–70% phase coverage that surpassed the intensity observed at 90% coverage, specifically reaching a maximum at 60%. Conversely, in the symmetric structure, the electric-field intensity at the focus decreased monotonically with respect to the phase coverage. At 90% phase coverage, no reduction was observed at 4 μm, whereas values below 1 were observed near 6 μm. As the phase coverage decreased to 60%, the reduction near the 4 μm wavelength became more pronounced. This enhancement of the spectral dip at 4 μm is considered to contribute to the improved focusing efficiency at a wavelength of 5 μm.

3.5 | Fabricated Metalenses

Figure 5 shows the GDSII CAD design of the radiative metalens with focal lengths of 5, 7.5, and 10 mm, and the mask for the metalens of final diameter 1 mm to highlight the concentric structure. As the focal length increases, the diameter of the concentric circles also increases. The structures were fabricated using the e-beam definition of the pattern into AR-P 6200 resist. The metalens was defined by a disc of meta-atoms forming the Fresnel lens, where a single zone had a 2π span of the phase across it. The entire metalens was successfully generated for the designed 1 mm-sized area in GDSII format. For the experimental measurements of thermal radiation, a still-larger metalens area is required. The size from 1 mm according to the phase Equation (1) was extended to the 5 mm phase mapping with the final number of concentric rings $N = 119$ ($f = 5$ mm), 81 ($f = 7.5$ mm), and 62 ($f = 10$ mm).

Figure S7 shows scanning electron microscopy (SEM) micrographs of the fabricated metasurface, highlighting the structural configuration of a single period of the outer ring. Although the architecture incorporated a full 2π phase coverage, the SEM images confirm high-fidelity fabrication within this region. The observed diameters of the circular resonators deviated from the design parameters by only 10–50 nm, demonstrating high fabrication precision with a dimensional tolerance of less than 0.5%. The measured reflection spectra for the 2π phase range at the central portion are presented in Figure S8. The objective of this study was to modulate the emission phase by varying the disc diameters of the meta-atoms. Ideally, a discrete meta-atom designed for a zero-emission phase should exhibit a reflectance dip approaching zero at a wavelength of 5 μm. However, because modifying the structural dimensions inherently shifts the resonant center wavelength, the collective reflection spectrum becomes an ensemble average of the individual spectra from meta-atoms of varying sizes. Consequently, the minimum reflectance degraded to ≈60%, resulting in a corresponding decrease in emissivity from the ideal unity (perfect emission). It is further inferred that the emissivity fluctuated among individual meta-atoms. These suboptimal characteristics led to a reduction in the overall focusing efficiency. We anticipate that significantly higher focusing efficiencies could be achieved if the phase could be modulated independently while maintaining a uniform 100% emissivity across all constituent meta-atoms.

3.6 | Focusing of Radiative Emission From the Metasurface: Experimental Verification

Figure 6 shows the experimentally measured radiation pattern obtained using the setup shown in Figure 2. The central region with the white-saturated region inside the color map is where the maximum intensity was located. The regions indicated in white represent peak intensities of ≈42. While the dynamic range of the measurement equipment is sufficient for these levels, displaying peak positions in red within the standard colormap would hinder visual discrimination. Therefore, to enhance clarity, the upper limit of the colormap was set to 40, and values exceeding this

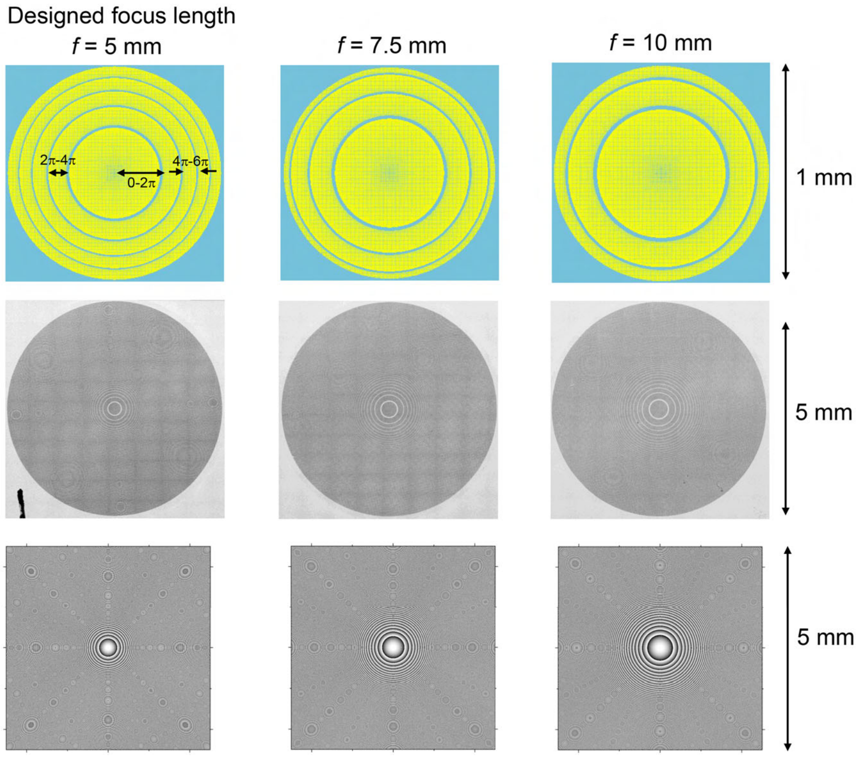

FIGURE 5 | GDSII file of the radiative metasurface with f = 5, 7.5, 10 mm for the 1 mm-diameter design (top row). Optical micrographic images of fabricated metalenses; an e-beam was used to define the final size meta-lenses of 5-mm diameter (middle row). Phase mapping using the spherical lens equation, Equation (1) (bottom row). The number of concentric phase rings is $N = 119$, 81, and 62, respectively.

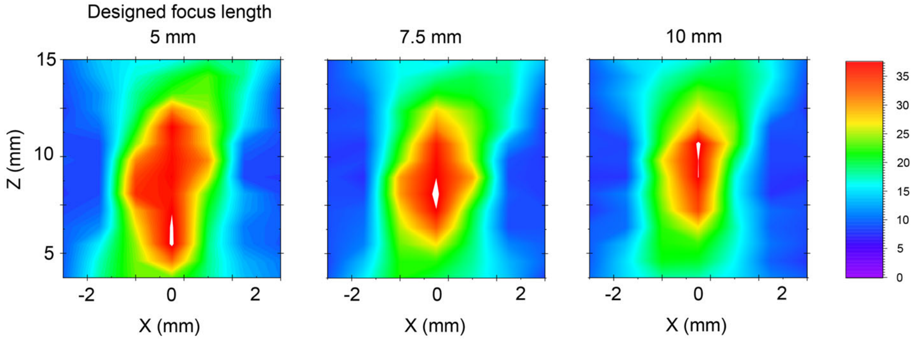

FIGURE 6 | Experimental thermal radiation mapping of intensity at the focal region (along the propagation direction) for the metalenses with focal length f = 5, 7.5, and 10 mm at $\lambda = 5$ µm. The scale bar is $|E|$; focal cross-section maps were measured over 7 × 14 points using the setup shown in Figure 2. The central region with the white-saturated area inside the color map is where the maximum intensity was located.

threshold are rendered in white. The position of the intensity maxima agreed closely with the designed focal point values f = 5, 7.5, and 10 mm. The spot size of x and z was 1.5/4.2 mm for $f = 5.0$ mm focal length, 1.9/2.4 mm for $f = 7.5$ mm, and 1.6/3.1 mm for $f = 10$ mm. However, the light focusing at $\lambda = 5$ µm was found to be extended over the region $1 \times 2\,\text{mm}^2$ near the focal position. This result was partially caused by a spectrally broad illumination spectrum over $\Delta\lambda \sim 700$ nm with a favorable phase condition for good focusing (Figure 3). The normal MIM metasurface, which had a uniform meta-atom size, was also measured for thermal radiation pattern for the reference. The result is shown in Figure S9, showing that focusing was not observed from the uniform MIM metasurface. The focusing efficiency was evaluated by comparing the gain coefficient of the focal peak intensity relative to the radiation intensity of a flat MIM surface. As shown in Figure S9, a 1.54-fold increase (from 27.5 to 42.5) was observed experimentally. Additionally, a background radiation value of ≈20 was measured, suggesting that the actual focusing gain may be higher than the calculated value. In contrast, FDTD simulations showed a 7.78-fold increase (from 0.80 to 6.25). This discrepancy is attributed to the fact that the simulation evaluates changes in reflection, whereas the experiment measures thermal radiation. Regarding thermal radiation, the metasurface optimized for 5 µm exhibits high radiation efficiency across the entire structure, although it lacks inherent directivity. Improving the overall radiation efficiency is therefore directly linked to enhancing the focusing efficiency.

3.7 | Influence of Coherence on Focusing by a Metalens

In this experiment, focusing of radiation from the MIM surface by a metalens was confirmed. However, the question remains whether the thermal radiation from the metasurface was coherent, because thermal radiation, including blackbody radiation, is inherently incoherent. To assess the effect of coherence on the metasurface radiation, FDTD calculations were performed using a plane-wave source, that is, all meta-atoms were in-phase for illumination and reflection. This condition implies a coherent light-metasurface interaction. However, it is reasonable to consider a situation in which the thermal radiation from each meta-atom is not in the ideal coherent state (in-phase). Indeed, thermal radiation based on black-body emission is known as a source of incoherent light. It has been reported that the transmission type of a metalens can focus an incoherent light source [7]. Therefore, it is essential to know how the coherence affects the performance of a Fresnel meta-lens fabricated with a MIM metasurface.

Figure 7 shows the FDTD simulation of the full metalens, which was defined by an array of 760 meta-atoms. Each meta-atom had either a dipole or total-field scattered-field (TFSF) light source. These two types of light sources provide an approach to defining the local excitation. The other sources, such as plane wave or Gaussian, would require expansion of the simulation region to be the same as the FDTD domain, which is prohibitively expensive because of memory requirements. All dipole sources have the same polarization, but the radiation phase is random. The TFSF sources have random polarization and are all in the same phase.

The optical phase was randomly modified from 0 to $\Delta\phi$, where $\Delta\phi = 60°, 120°, 180°$. In the case of coherent interaction, the phase distribution was at 0° and the results for the dipole and TFSF were well matched. By design, the light was focused along the axial extension from 60 to 80 µm. The focusing intensity decreased with an increase in the randomness of the polarization and phase (bottom row in Figure 7). Interestingly, the focusing performance remained even for the 0°–120° randomness in the phase distribution. On the other hand, it almost disappeared for the 0°–180° condition. These results corroborate that a focus still exists even if the source is not entirely coherent.

Studies on transparent (at visible spectral range) electrically conducting films reported that metalenses work with laser (coherent) as well as LED (incoherent) illumination [7]. The relationship between the degree of randomness and electric-field intensity at the focus is illustrated in Figure 8. In the range of randomness for the 0°–120° phases, the focal intensity decreased slightly but remained above 80%. When randomness was beyond 150°, however, the intensity dropped abruptly. Despite the linear fit shown in Figure 8, the actual data exhibited an oscillating downward trend (not captured by the sparse data sampling shown in Figure 8). This fluctuation likely depends on the specific phase values assigned to individual structures. Although a more precise assessment using mean and variance from various phase configurations is necessary for a comprehensive analysis, the present results sufficiently demonstrate the overall trend.

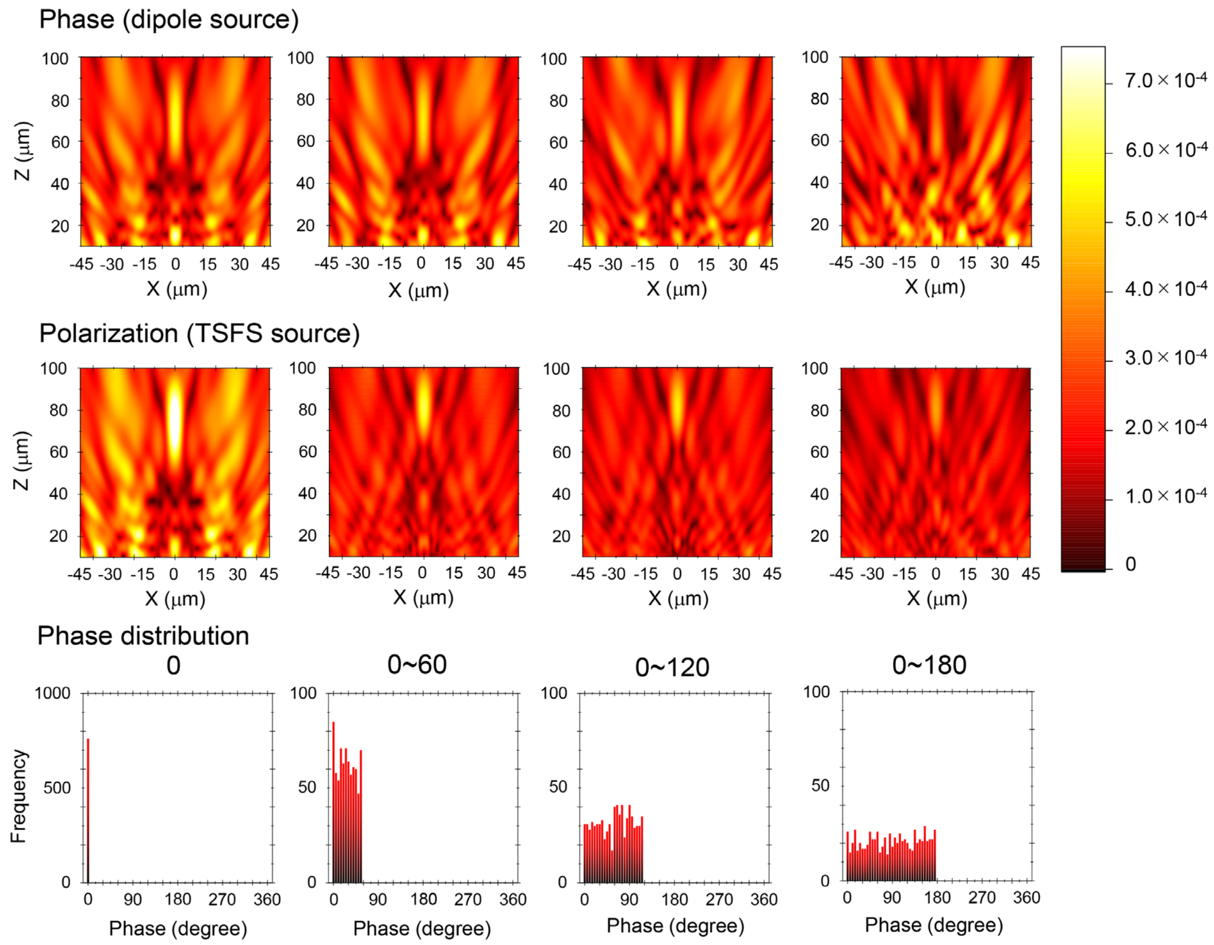

FIGURE 7 | FDTD simulation of axial intensity distribution for the dipole and TFSF sources under a 760 meta-atom design. The dipole sources have the same polarization and random phase, whereas the TFSF source has random polarization but the same phase. The same random angle was used between TFSF and dipole. E-field intensity was normalized by the number of light sources, 760.

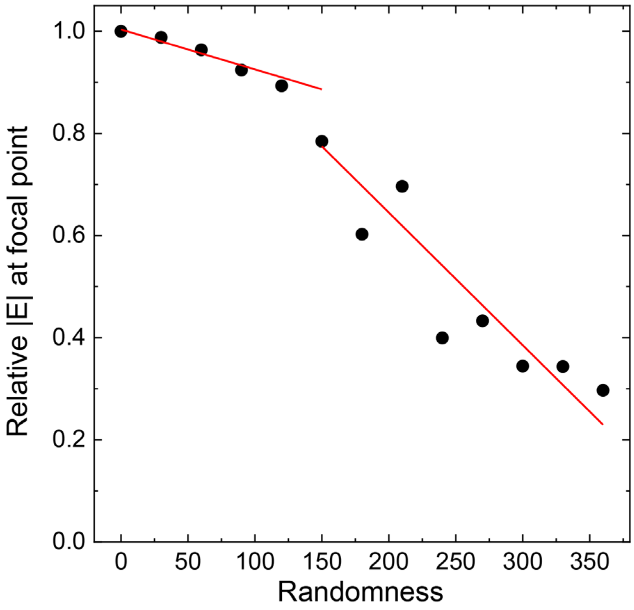

FIGURE 8 | Plot of $|E|$ at the focal point in Figure 7. The data were normalized to the condition were the randomness was zero, that is, a coherent condition. The red line is the least square in the ranges 0°–120° and 120°–360°.

4 | Conclusion and Outlook

In this study, we experimentally demonstrated focusing of thermal radiation using a Fresnel metalens formed using a MIM metasurface. FDTD simulation results reveal that focusing existed even at not entirely coherent conditions of the emitting surface. However, the focusing was most efficient for coherent (in-phase) radiation. These findings form the basis for the engineering of metasurfaces for focusing thermal radiation. Such surfaces can perform at antireflection (perfect emitter) conditions and, consequently, have the function of thermal radiation extraction.

The proposed method of thermal radiation extraction by focusing using engineered surface textures can prove useful for the IR wavelength-specific light sources in gas sensors, harvesting of thermal energy, antiradar in defense applications, and radiation cooling, especially for semiconductor devices such as CPUs, GPUs, and storage memory banks operating at elevated temperatures.

Author Contributions

Tsuyoshi Kawaida: data curation (equal), formal analysis (equal), investigation (equal). **Kazuki Wada:** data curation (equal), formal analysis (equal). **Kazuma Sekiya:** data curation (equal), formal analysis (equal), software (lead). **Megumi Tanaka:** data curation (equal), formal analysis (equal). **Thoko Ogata:** formal analysis (equal), investigation (equal). **Yasutaka Matsuo:** investigation (equal), methodology (equal), resources (equal), writing – original draft (equal). **Saulius Juodkazis:** formal analysis (equal), funding acquisition (equal), methodology (equal), writing – original draft (lead). **Yoshiaki Nishijima:** conceptualization (lead), data curation (equal), funding acquisition (lead), investigation (equal), methodology (equal), project administration (lead), writing – original draft (equal).

Acknowledgments

S. J. is grateful for the research stays at Yokohama National University and Vilnius University.

Open access publishing facilitated by Swinburne University of Technology, as part of the Wiley - Swinburne University of Technology agreement via the Council of Australasian University Librarians.

Funding

Y. N. is grateful for partial support from the Japan Society for the Promotion of Science (JSPS), Grants-in-Aid for Scientific Research, JSPS Bilateral Joint Research Projects between Japan and Lithuania. This work was partially supported by PRESTO, the Japan Science and Technology Agency (JST) (JPMJPR22B6). ARIM of MEXT in Japan supported a part of this work via grant JPMXP1223HK0070 executed under the Cooperative Research Program of the Network Joint Research Center for Materials and Devices (MEXT).

Conflicts of Interest

The authors declare no conflicts of interest.

Data Availability Statement

Data underlying the results presented in this paper are not publicly available but may be obtained from the authors upon reasonable request.

References

1. Y. Matsuoka, S. Mathonnèire, S. Peters, and W. T. Masselink, "Broadband Multilayer Anti-Reflection Coating for Mid-Infrared Range From 7 μm to 12 μm," *Applied Optics* 57, no. 7 (2018): 1645–1649.

2. Q. Chen, Y. Gao, S. Pian, and Y. Ma, "Theory and Fundamental Limit of Quasiachromatic Metalens by Phase Delay Extension," *Physical Review Letters* 131, no. 19 (2023): 193801.

3. W. T. Chen, A. Y. Zhu, V. Sanjeev, et al., "A Broadband Achromatic Metalens for Focusing and Imaging in the Visible," *Nature Nanotechnology* 13, no. 3 (2018): 220–226.

4. X. Chen, L. Huang, H. Mühlenbernd, et al., "Dual-Polarity Plasmonic Metalens for Visible Light," *Nature Communications* 3 (2012), 1198.

5. L. Huang, Z. Coppens, K. Hallman, et al., "Long Wavelength Infrared Imaging under Ambient Thermal Radiation via an All-Silicon Metalens," *Optical Materials Express* 11, no. 9 (2021): 2907.

6. N. Ishizuka, J. Li, W. Fuji, S. Ikezawa, and K. Iwami, "Linear Polarization-Separating Metalens at Long-Wavelength Infrared," *Optics Express* 31, no. 7 (2023): 23372.

7. K. Iwami, C. Ogawa, T. Nagase, and S. Ikezawa, "Demonstration of Focal Length Tuning by Rotational Varifocal Moiré Metalens in an Ir-a Wavelength," *Optics Express* 28, no. 11 (2020): 35602.

8. S. J. Kim, C. Kim, Y. Kim, et al., "Dielectric Metalens: Properties and Three-Dimensional Imaging Applications," *Sensors* 21 (2021): 4584.

9. B. Li, W. Piyawattanametha, and Z. Qiu, "Metalens-Based Miniaturized Optical Systems," *Micromachines* 10, no. 5 (2019): 310.

10. W. Liu, H. Cheng, J. Tian, and S. Chen, "Diffractive Metalens: From Fundamentals, Practical Applications to Current Trends," *Advances in Physics: X* 5, no. 1 (2020): 1742584.

11. X. Luo, "Plasmonic Metalens for Nanofabrication," *National Science Review* 5, no. 3 (2018): 137–138.

12. R. Paniagua-Domínguez, Y. F. Yu, E. Khaidarov, et al., "A Metalens with a Near-Unity Numerical Aperture," *Nano Letters* 18, no. 3 (2018): 2124–2132.

13. D. Sang, M. Xu, M. Pu, et al., "Toward High-Efficiency Ultrahigh Numerical Aperture Freeform Metalens: From Vector Diffraction Theory to Topology Optimization," *Laser and Photonics Reviews* 16, no. 10 (2022), 2200265.

14. M. L. Tseng, H. H. Hsiao, C. H. Chu, et al., "Metalenses: Advances and Applications," *Advanced Optical Materials* 6, no. 18 (2018): 1800554.

15. S. Wang, L. Li, S. Wen, et al., "Metalens for Accelerated Optoelectronic Edge Detection under Ambient Illumination," *Nano Letters* 24, no. 1 (2024): 356–361.

16. D. Wintz, P. Genevet, A. Ambrosio, A. Woolf, and F. Capasso, "Holographic Metalens for Switchable Focusing of Surface Plasmons," *Nano Letters* 15, no. 5 (2015): 3585–3589.

17. R. Yamada, H. Kishida, T. Takami, et al., "Optical Fresnel Zone Plate Flat Lenses Made Entirely of Colored Photoresist through an i-Line Stepper," *Light: Science and Applications* 14 (2025): 43.

18. R. Dharmavarapu, S. H. Ng, F. Eftekhari, S. Juodkazis, and S. Bhattacharya, "Metaoptics: Opensource Software for Designing Metasurface Optical Element Gdsii Layouts," *Optics Express* 28, no. 3 (2020): 3505–3516.

19. D. R. Smith, D. C. Vier, T. Koschny, and C. M. Soukoulis, "Electromagnetic Parameter Retrieval From Inhomogeneous Metamaterials," *Physical Review E* 71, no. 7 (2005): 036617.

20. Z. Szabó, G.-H. Park, R. Hedge, and E.-P. Li, "A Unique Extraction of Metamaterial Parameters Based on Kramers-Kronig Relationship," *IEEE MTT* 58 (2010): 2646–2653.

Supporting Information

Additional supporting information can be found online in the Supporting Information section. **Supporting Fig. S1:** (a) Chromatic abberration of MIM metalens. The X–Z field image from 4 to 6 μm wavelength. Light propagation direction is along z-axis. (b) Phase and reflection plot at wavelength of 4.0, 4.5, 5.0, 5.5, 6.0 μm. **Supporting Fig. S2:** Focusing behavior of plane wave and Gaussian beam illumination. The focusing becomes stronger when FWHM of the Gauss beam has increased. The FWHM = $3D$ condition is almost same as the plane wave excitation; D is the beam diameter. **Supporting Fig. S3:** Focusing behavior with different phase coverage range and with asymmetry coverage range. **Supporting Fig. S4:** Focusing behavior with different phase coverage range with a symmetric phase coverage. **Supporting Fig. S5:** Focusing field intensity with asymmetric and symmetric phase coverage and their corresponding CAD design used for FDTD simulations. **Supporting Fig. S6:** Reflection intensity (in arb. units) obtained at the focal length at different phase coverage ranges: asymmetric and symmetric. **Supporting Fig. S7:** SEM image of a segment of fabricated metalens. The disk diameters were below ±20 nm precision from the designed size. Small white dots are caused by dust that was attached to the surface during measurements. **Supporting Fig. S8:** Optical Reflection (normalised) spectra of a metalens that include disks for the full phase coverage range from 0 to 2π. **Supporting Fig. S9:** Comparison of radiation patterns from the uniform MIM metalens and uniform MIM metasurface with experiments (top-row) and FDTD simulations (bottom-row).